

# Design and demonstration of a miniature catheter for a confocal microendoscope

Andrew R. Rouse, Angelique Kano, Joshua A. Udovich, Shona M. Kroto, and Arthur F. Gmitro

The fluorescence confocal microendoscope provides high-resolution, *in vivo* imaging of cellular pathology during optical biopsy. The confocal microendoscope employs a flexible fiber-optic catheter coupled to a custom-built slit-scan confocal microscope. The catheter consists of a fiber-optic imaging bundle linked to a miniature objective and focus assembly. The 3-mm-diameter catheter may be used on its own or routed through the instrument channel of a commercial endoscope, adding microscopic imaging capability to conventional endoscopy. The design and performance of the miniature objective and focus assembly are discussed. Primary applications of the system include diagnosis of disease in the gastrointestinal tract and female reproductive system. © 2004 Optical Society of America

OCIS codes: 170.1790, 170.2150, 170.2520, 170.3880, 170.6900.

## 1. Introduction

Cancer is the second leading cause of death in the United States. With current technology, the time between onset of disease and detection of cancer is often ten or more years. Since cancer becomes more difficult to treat as it develops, it is crucial to detect and diagnose the disease as early as possible.<sup>1</sup>

Traditional biopsy methods for diagnosis of disease are surgically invasive and require significant turnaround time for results. Often the patient has to return for additional biopsies. Also, there is the risk that the specific location of the disease may be overlooked owing to the inherent sampling nature of the procedure. Regular screening of easily accessible cancers such as those of the gastrointestinal track is rarely performed, in part because of the invasiveness of traditional biopsy procedures.<sup>1</sup>

Truly noninvasive imaging modalities such as magnetic resonance imaging and computed tomography have the ability to image the entire body but do not have the resolution required for visualizing the morphological and cellular changes of early stage cancer and precancer. Optical biopsy is a relatively

new technique that strives to provide the physician with real-time cellular imaging from a minimally invasive endoscopic procedure. Conventional microscopy has limited utility if the thick biological tissues to be viewed are thick. Light returned from out-of-focus regions in the sample overlaps the in-plane information, causing a significant reduction in image quality. Confocal microscopes<sup>2,3</sup> are commonly used to investigate thick excised biological tissue samples because these instruments reject light from out-of-focus planes and provide high-quality images from within a localized region of the tissue. Confocal microscopes typically can capture high-resolution images from a specific plane in the tissue up to a few hundred micrometers below the surface. Since most cancers are epithelial,<sup>1</sup> the confocal microscope is an excellent choice for optical biopsy.

Confocal microscopes have been adapted for *in vivo* imaging of the skin,<sup>4,5</sup> cornea,<sup>6,7</sup> teeth,<sup>8</sup> and cervix.<sup>9</sup> Specialized endoscopic systems based on vertical-cavity surface-emitting laser arrays,<sup>10</sup> micromachined scan mirrors,<sup>11</sup> single optical fibers,<sup>12,13</sup> and fiber-optic bundles<sup>14,15</sup> have been developed for imaging deeper within the body.

We have developed and previously reported on a confocal microendoscope capable of high-resolution *in vivo* microscopic visualization of tissue.<sup>16–18</sup> Here we report on an improved system that employs a flexible fiber-optic catheter with a maximum outside diameter of 3 mm. The small size of the catheter makes remote locations in the body accessible to the confocal microendoscope. In addition to working as

---

The authors are with the Optical Science Center and the Department of Radiology, University of Arizona, Tucson, Arizona 85724. A. Gmitro's e-mail address is gmitro@radiology.arizona.edu.

Received 11 February 2004; accepted 17 May 2004.

0003-6935/04/315763-09\$15.00/0

© 2004 Optical Society of America

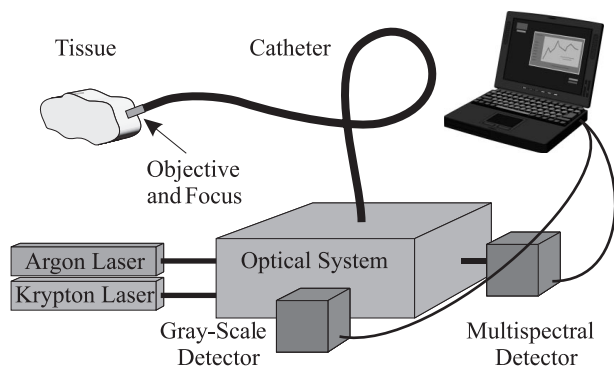


Fig. 1. Functional components of the slit-scan confocal microendoscope.

a stand-alone product, the catheter is sufficiently small to be used as a daughter scope to a conventional endoscope. Commercial endoscopes often incorporate empty instrument channels that enable the clinician to use the endoscope to guide additional instrumentation to the site of the disease. The small size of the catheter permits the confocal microendoscope to be used in conjunction with the highly developed technology that is currently used routinely in medical endoscopy procedures.

## 2. System Description

Figure 1 depicts the general layout and operation of the confocal microendoscope. A detailed explanation of the bench-top portion of the confocal microendoscope has been described in previous publications.<sup>17,18</sup> Briefly, the system consists of scanning optics, an illumination arm, a fiber-optic catheter, and a detection arm. The illumination arm incorporates argon-ion and krypton-ion lasers, which can provide various excitation wavelengths throughout the ultraviolet and visible spectrum. The 488-nm argon-ion and the 647.1-nm krypton-ion laser lines are the most commonly used. An anamorphic optical system shapes the laser profiles into a line of illumination that is scanned in one dimension across the proximal face of the catheter. A slit-scanning system was chosen over the more conventional point-scanning system to speed up image-acquisition rates. Near video rate imaging is important when one dynamically views tissues during *in vivo* experiments.

The catheter incorporates a fiber-optic imaging bundle from Sumitomo Electric<sup>19</sup> (IGN 08/30) that transfers the scanned illumination profile to the distal (*in vivo*) end of the catheter. The fiber measures 1 mm in overall diameter and contains 30,000 optical elements with 3- $\mu\text{m}$  center-to-center spacing. A miniature achromatic objective images the distal end of the fiber bundle into the tissue, and a miniature focus mechanism allows for focus control to 200  $\mu\text{m}$  below the surface of the tissue. Specific details of the distal optomechanical assembly are discussed in the following section.

Induced sample fluorescence is collected by the distal optics and relayed back through the catheter. A

dichroic beam splitter reflects the fluorescence onto a confocal slit aperture located in the detection arm. The dichroic beam splitter is interchangeable, allowing the user to tailor the system to the specific excitation and emission characteristics of the fluorescent probe. Energy passed by the slit aperture is directed into either gray-scale or multispectral collection systems. The specific details of each of these collection methods may be found in previous publications.<sup>17,18</sup>

## 3. Catheter Design and Performance

The catheter presented in this paper is the second generation for the confocal microendoscope. The primary development goal was to reduce its diameter and thus broaden its practical application to *in vivo* medical diagnosis. The 7-mm-diameter first-generation catheter is small and flexible relative to commercial bench-top confocal microscopes; however, further miniaturization of the catheter dramatically increases the confocal microendoscope's clinical utility. Clearly, a smaller catheter permits imaging of remote locations not accessible by the first-generation design.

As stated in Section 1, development of a sufficiently small and flexible catheter also allows the confocal microendoscope to be used as a daughter scope to clinical endoscopes. For example, an Olympus CF-100L colonoscope has an empty 3.2-mm-diameter instrument channel. To insure the smooth operation of the confocal microendoscope in this instrument channel, we restricted the new catheter to a maximum diameter of 3.0 mm with a rigid optomechanical distal assembly shorter than 25 mm.

By design, the catheter must incorporate a high-quality objective lens to image the distal face of the fiber bundle into the tissue. The catheter also requires a reliable method by which to control the image depth in the tissue. In the following sections the design, fabrication, and performance of each of these subassemblies are described.

### A. Miniature Objective Design

The miniature objective serves two purposes. First, it transfers the illumination profile from the distal tip of the fiber bundle into the tissue. Second, it collects the fluorescence excited in the tissue and images this energy back onto the distal tip of the fiber bundle. Since light travels both ways through the lens, the terms tissue space and fiber space will be used in place of the usual object and image space nomenclature.

The general optical properties and the requirements on the imaging performance for the lens are summarized in Table 1. Many of the optical properties of the lens were chosen to match specific properties of the fiber-optic imaging bundle. To reduce the likelihood of cross talk between individual pixels of the fiber bundle, we chose a fiber side numerical aperture (NA) of 0.29 that slightly underfills the fiber bundle NA of 0.35. The lens has a nominal magnification of 1.6 from tissue to fiber. The NA and field

**Table 1. Specification of the 3-mm-Diameter Objective**

| Specification                    | Value                      |
|----------------------------------|----------------------------|
| Magnification (tissue to fiber)  | 1.6                        |
| Full field of view in tissue     | 450 $\mu\text{m}$          |
| NA in fiber space                | 0.29                       |
| NA in tissue space               | 0.46                       |
| Refractive index in tissue space | Water                      |
| MTF at 166 lp/mm at fiber        | >50%                       |
| Rms spot size at fiber           | <3- $\mu\text{m}$ diameter |
| Telecentric in tissue space      | Yes                        |
| Telecentric in fiber space       | Yes                        |
| Nominal focal distance in tissue | 25 $\mu\text{m}$           |
| Range of focus in tissue         | 0 to 200 $\mu\text{m}$     |
| Focus compensator                | Fiber position             |
| Achromatic range                 | 480–660 nm                 |
| Packaged diameter                | $\leq 3$ mm                |
| Packaged length                  | $\leq 13$ mm               |

of view in the tissue are determined by the magnification and the characteristics of the fiber bundle.

One of the principal design goals for the lens was to achieve a modulation transfer function (MTF) contrast at the fiber plane greater than 50% at 166 lp/mm. This spatial frequency corresponds to the maximum fiber plane spatial frequency that will not be aliased by the 3- $\mu\text{m}$  sampling period (center-to-center spacing) of the fiber bundle. A minimum contrast of roughly 50% at this frequency ensures that the lateral resolution of the system is not limited by the performance of the objective lens but rather by the inherent resolution characteristics of the fiber bundle.

As with most microscope objectives, the lens system is roughly telecentric in tissue space to minimize the change in magnification with respect to focal position. Unlike traditional microscope objectives, the lens is also telecentric in fiber space. If the lens were not telecentric in fiber space, some light incident on the fiber near the edge of the field would exceed the acceptance angle (NA) of the fiber bundle. Telecentricity in fiber space ensures uniform fiber coupling efficiency across the entire field of view.

The objective is corrected for chromatic aberrations over the spectral range from 480 to 660 nm, which allows the system to be used with a broad range of fluorophors while still maintaining adequate imaging performance. It also permits the simultaneous use of multiple dyes with multiple excitation and emission profiles. This chromatic correction is particularly important during operation in the multispectral mode in which the confocal microendoscope is essentially acting as an imaging spectrometer. In such a configuration, it is vital that the measured spectra accurately correlate to a spatial location in the tissue, a property that depends on appropriately correcting chromatic aberrations in the lens.

The miniature focus mechanism described in the next section screws directly onto the miniature objective to form a seamless optomechanical assembly. The focus mechanism moves the position of the fiber with respect to the objective and therefore provides

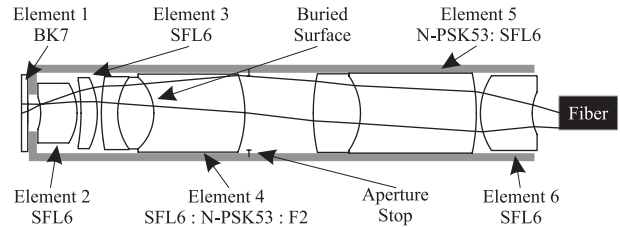


Fig. 2. Schematic of the 3-mm-diameter objective lens. The tissue plane is on the left.

the ability to adjust the focal depth in the tissue. When assembled, the objective and focus mechanism allow focus control to a depth of 200  $\mu\text{m}$  in the tissue. The objective must be designed to perform adequately for conjugates throughout this focal range.

Extensive work was done to design a lens to meet the specifications listed in Table 1. The final design, depicted in Fig. 2, consists of 6 elements with 13 surfaces that impart optical power. Element 1 is a microscope coverslip that is glued on the exterior face of the lens barrel. The coverslip protects the lens from moisture and abuse and is easy to replace when it gets excessively dirty or scratched. The physical length of the fabricated lens is less than 13 mm.

To arrive at the solution depicted in Fig. 2, we used the concept of buried achromatizing surfaces.<sup>20,21</sup> This technique is based on the selection of a pair of glasses that have nearly identical refractive indices but significantly different dispersions. Since there is no change in index of refraction across the buried surface, the designer can vary the curvature and position of the surface without altering the monochromatic performance of the lens. In theory, a well-corrected monochromatic design can be achromatized with no effect on the original monochromatic performance. In practice, it is difficult to attain sufficient achromatization without altering the monochromatic solution slightly. However, the technique is still a useful tool for reducing the complexity of the initial design process. N-PSK53 and F2 were used as the buried surface glasses for this design.

To further simplify the design process, the higher NA tissue half of the lens (elements 1–4) was designed independently of the fiber half of the lens (elements 5–6). The monochromatic solution for the tissue half of the lens consisted of the coverslip (element 1), two singlets (elements 2 and 3), and a doublet (element 4) with SFL6 and N-PSK53 glasses. Once a monochromatic solution to the tissue half of the lens was realized, a starting condition for the fiber half of the system was obtained by simply replicating and scaling the tissue half solution. The two sections were then merged and further optimized to achieve a final monochromatic solution for the objective.

To achromatize the lens, each of the N-PSK53 glass spaces were split into N-PSK53 and F2 regions. This splitting formed a triplet on either side of the aperture stop, each incorporating one buried surface. The lens system was then reoptimized over the full

spectral range. As a final solution was achieved, it was found that the fiber half of the lens could be reduced from a triplet and two singlets to a doublet and one singlet without sacrificing image quality.

During the design process, field curvature was one of the aberrations that significantly limited the optical performance of the lens. In effect, this means that the fiber plane is mapped to a spherical surface inside the tissue. Since there is a one-to-one mapping between this spherical surface and the flat distal face of the fiber bundle, the practical result of field curvature is that the optical section in the tissue lies on a spherical surface rather than on a plane. Since the confocal microendoscope is used to image thick biological tissue samples, a small amount of field curvature is not a problem. In the design process, we relaxed the correction for field curvature by optimizing and evaluating the lens, assuming a slightly curved tissue plane with a radius of 4 mm. This radius corresponds to a sag of 6  $\mu\text{m}$  at the edge of the field, which is less than the predicted axial resolution of the confocal microendoscope.

A rigorous tolerance analysis was performed on the design to confirm that the miniature objective was not overly sensitive to fabrication errors, to alignment errors, or to both. A Monte Carlo simulation was performed to estimate the combined effects of all the fabrication and alignment tolerances. The analysis and simulations predicted that a lens with adequate performance could be fabricated to the specifications listed in Table 1. The lens shown in Fig. 2 was fabricated and assembled by Optics Technology.<sup>22</sup>

#### B. Miniature Objective Performance

An ultra-high-resolution air force bar target was used to test the optical performance of the fabricated lens. It is possible to sample the MTF of the miniature objective by measuring the degradation in the spatial frequency patterns of the bar target. The bar target was placed in tissue space and illuminated with incoherent white light spectrally limited by an 80-nm bandpass filter centered at 560 nm. This filter has appreciable transmission over most of the operating spectral range of the miniature objective. A diffuser was placed between the light source and the bar target to insure uniform illumination over the full NA of the miniature objective. The target was placed 19  $\mu\text{m}$  away from the exterior surface of the miniature objective's coverslip (element 1). In the test setup, the space between the bar target and the coverslip was air. Assuming an index of refraction for tissue similar to that of water (1.33), it follows that the 19- $\mu\text{m}$  air space corresponds to a depth of approximately 25  $\mu\text{m}$  in tissue.

The contrast measurements required frequent repositioning of the target, which made water coupling impractical. Since the miniature objective was designed for water immersion, the air space between the bar target and the objective introduces a small amount of additional spherical aberration. If the miniature objective performs adequately in air, it

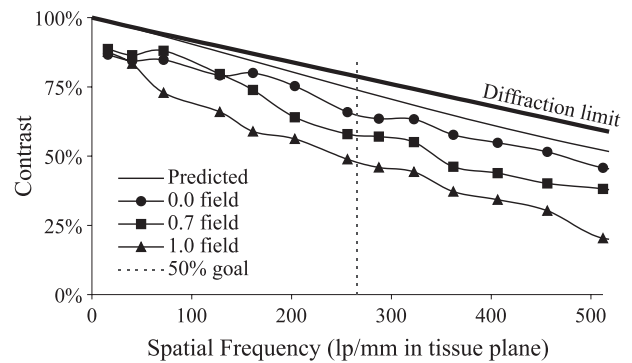


Fig. 3. Measured and predicted MTF of the miniature objective (bar target test). The vertical dotted line represents the spatial frequency at which a minimum of 50% contrast was required.

should perform better when in contact with tissue. We verified this supposition by taking several measurements with and without water coupling and observed a slight increase in contrast in the water-coupled images.

We sampled the MTF of the lens by measuring the contrast in the image of the bar target for various spatial frequencies. An identical procedure was used to calculate the MTF of the optical measurement system without the miniature objective present. The true MTF of the miniature objective was obtained by division of the MTF of the whole system (lens plus measurement optics) by that of the optical measurement system alone.

Figure 3 shows the MTF results for three field positions: on axis, 70% off axis, and at full field. The contrast measurements are the average of the horizontal and the vertical bar-target patterns for each frequency. The thick solid line shows the on-axis diffraction-limited performance for the miniature objective. The thin solid line is the predicted MTF of the lens, averaged over all fields, assuming no fabrication or assembly errors. The data are presented in terms of tissue plane spatial frequency. The vertical dashed line represents a tissue plane spatial frequency of 266 lp/mm, which corresponds to the test spatial frequency, stated in Table 1, of 166 lp/mm at the fiber plane. These results show a minimum contrast of 50% over the entire field at the test frequency.

At very low spatial frequencies, the MTF curves in Fig. 3 converge to a common average MTF for all fields. The low spatial frequency features of the bar target are quite large with respect to the field of view of the miniature objective, which makes it difficult to measure the contrast at a discrete field position. Therefore, the first data point in Fig. 3, which corresponds to the lowest spatial frequency that could be sampled by the test setup, should be viewed as an average MTF over all fields. The contrast is slightly lower than one might expect at the lowest spatial frequencies presumably owing to imperfect coatings that cause a small amount of diffuse stray light in the images. However, this performance reduction is not noticeable under normal operating conditions.

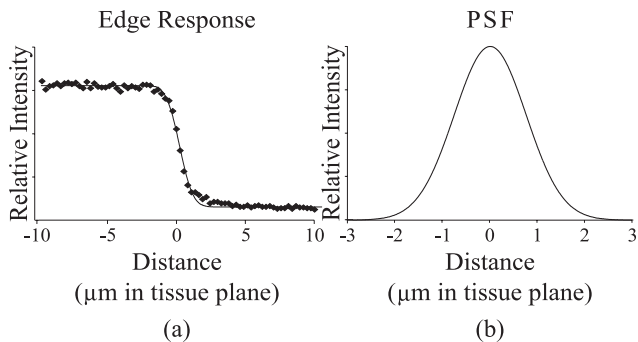


Fig. 4. Measured lateral resolution of the miniature objective (knife-edge test). (a) Edge response with cumulative Gaussian distribution fit and (b) the corresponding Gaussian approximation to the PSF.

A simple edge-response test was used as an additional verification of lateral resolution for the miniature objective lens. The bar target was positioned such that a large on-off region was centered in the field of view. A one-dimensional profile of this edge response is plotted in Fig. 4(a) along with an approximate fit to a cumulative Gaussian distribution. The derivative of this profile corresponds to the lateral point-spread function (PSF) for the lens<sup>23</sup> and is plotted in Fig. 4(b). The Gaussian shape of the PSF is only an estimate since the cumulative distribution used to fit the profile data is only an approximation. However, its overall form and width are adequate for lateral-resolution estimates. The lateral resolution of the miniature objective may be approximated by the full width-half at maximum (FWHM) of the PSF. The data presented in Fig. 4 indicates a FWHM of 1.8  $\mu\text{m}$  in tissue space. Accounting for magnification, this value corresponds to 2.88  $\mu\text{m}$  in fiber space, which implies that the lens can resolve the individual elements of the fiber bundle.

The lateral-resolution measurements described above suggest that the new 3-mm-diameter miniature objective will perform as well or better than the previous 7-mm-diameter design. The lateral and axial resolutions of the full system have not been characterized with the new objective. However, we expect the resolution to be nearly identical to that previously reported.<sup>17,18</sup>

We investigated the spectral performance of the lens by measuring the axial shift in the image plane for a fixed object of varying color. The high-resolution bar target was illuminated with a series of 10-nm-wide bandpass filters. The resultant axial shift in image-plane location was measured. These data were then divided by the square of the magnification of the miniature objective and scaled by the index of refraction of water to obtain the chromatic focal shift in tissue space. The results are compared with the predicted lens performance in Fig. 5. The data show a maximum image-plane focal shift of 6.5  $\mu\text{m}$  over the full chromatic range of the design, which is in close agreement with the predicted performance. Most fluorophors excite and emit within an 80-nm-

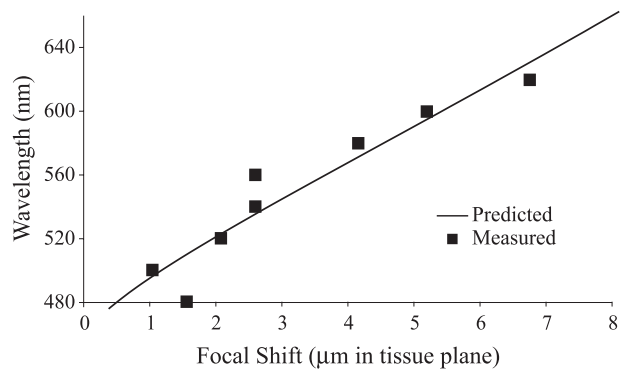


Fig. 5. Measured and predicted axial color of the miniature objective (focal shift in tissue space).

wide spectral bandwidth. The chromatic focal-shift data for the miniature objective indicate less than 3  $\mu\text{m}$  of axial color over this bandwidth.

### C. Pneumatic Focus Mechanism

The catheter for the confocal microendoscope employs a focusing system that can accurately control the axial position of the fiber bundle with respect to the miniature objective. This function enables the operator to change the imaging conditions for the objective and in effect, scan the focal position in the sample to a tissue depth of 200  $\mu\text{m}$ . Two separate focus mechanisms have been designed and fabricated, one pneumatic and the other mechanical.

Figure 6 shows the layout of the miniature pneumatic focus mechanism. The mechanism uses pressurized air to move the fiber with respect to the objective lens and consists of a miniature distal subassembly and a somewhat larger proximal subassembly. The focus system is based on a novel design that integrates the imaging fiber and pneumatic supply line into a single concentric unit. The fiber bundle is routed through semiflexible high-pressure tubing with an inside diameter of 1.6 mm and an outside diameter of 2 mm. This tubing runs the entire length of the catheter and delivers air to the distal optomechanical assembly while simultaneously providing an additional layer of protection to the fiber bundle.

The proximal subassembly serves as a means to introduce air pressure into the pneumatic tubing

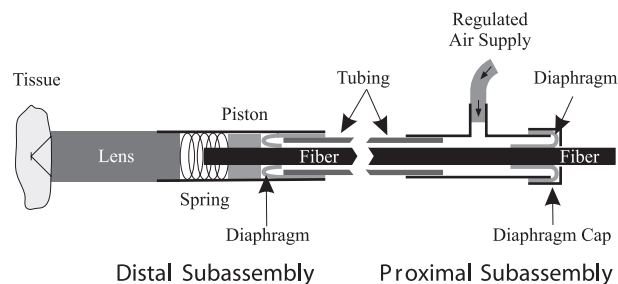


Fig. 6. Pneumatic focus assembly. Distal subassembly is shown screwed to the lens barrel. The fiber extends to the right and enters the bench-top optical system. (Drawing not to scale.)

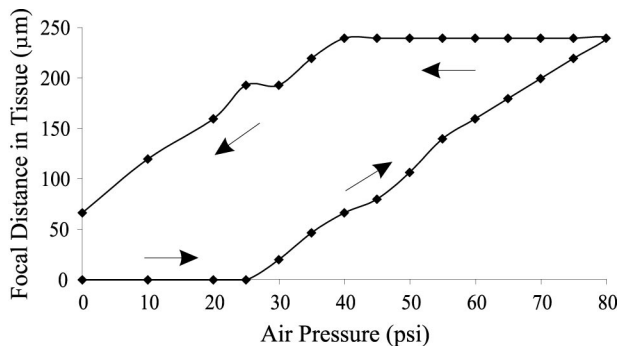


Fig. 7. Measured performance of the pneumatic focus mechanism.

while simultaneously allowing the fiber to move freely with respect to the tubing and proximal subassembly housing. A small cylindrical piece of latex manufactured by North American Latex,<sup>24</sup> acts as a diaphragm and allows the fiber to move with respect to the housing. The latex diaphragm is fitted tightly over the fiber, wrapped back over the housing, and held in place by a retaining cap. As air pressure is increased, the diaphragm in the proximal portion of the mechanism presses against the rigid walls of the end cap but does not produce an axial (focus) force on the fiber.

A similar concept is employed in the distal subassembly. A small cylindrical piece of latex acts as a diaphragm and allows the fiber to move with respect to the tubing and the distal subassembly housing. The latex is placed on the fiber bundle and then folded over the semiflexible pneumatic tubing. The tubing and latex diaphragm are then inserted into the metal casing of the focus mechanism. The fiber bundle is attached to a piston that is located between the latex diaphragm and the miniature objective. As air is introduced into the feed line via the proximal subassembly, the pressure causes the diaphragm to expand, and the piston and fiber are pushed toward the lens. A spring between the lens and the piston provides the restoring force necessary to push the piston and fiber away from the lens as air pressure is decreased. Once everything is assembled, the axial forces on the fiber come from the force applied to the piston through the diaphragm and through the restoring spring in the distal assembly. Focusing of the confocal microendoscope is accomplished by regulation of the air pressure in the catheter. The precision mechanical parts of the miniature focus mechanism were fabricated by Optics Technology.<sup>22</sup>

The assembled pneumatic focus mechanism was tested to characterize its functionality. Figure 7 shows the tissue-space imaging location versus air pressure. To collect these data, we slowly increased the air pressure from 0 to 80 psi and then decreased it back to 0 psi while tracking the imaging position in tissue space. The focal-plane measurements were taken in air and then scaled by the index of water (1.33) to estimate the depth of focus control in tissue. While the mechanism exhibits significant hysteresis,

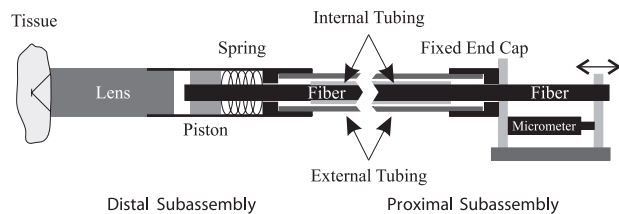


Fig. 8. Mechanical focus assembly. Distal subassembly is shown screwed to the lens barrel. The fiber extends to the right and enters the bench-top optical system. (Drawing not to scale.)

focal-plane positioning is fairly linear and quite repeatable. The backlash in the focus mechanism makes absolute positioning difficult. However, in practice, a trained user can quickly scan through the hysteresis region and obtain reliable relative focus control. The mechanism is unaffected by small air leaks because the position of the piston is based on pressure in the tube, not by the quantity of air introduced into the system. The focal position is stable over long periods and unaffected by small movements of the catheter. The lateral position of the image is extremely stable with respect to focus because of the tight tolerance between the piston and the interior wall of the housing. The pneumatic focus mechanism has been used successfully to image biological samples.

#### D. Mechanical Focus Mechanism

One of the major drawbacks to the pneumatic focus mechanism is the potential safety concern associated with the delivery of high-pressure gas. An alternative focus mechanism was developed that works on a principle similar to that of a bicycle brake cable. Figure 8 shows the layout of the system. The fiber is routed through semirigid tubing with an outside diameter of 2 mm. We achieved focus by mechanically moving the fiber with respect to the outer tubing. The proximal subassembly consists of a catheter end cap and a precision micrometer. The end cap is glued to the external tubing and is fixed to the optical bench. The bare fiber bundle is mounted to a translation stage controlled by a micrometer, which allows the user to move the fiber bundle with respect to the external tubing and proximal end cap.

In the distal subassembly, the external tubing is fixed to the housing of the focus mechanism. The external tubing provides an axially rigid structure between the proximal and the distal subassemblies. As the fiber is retracted by the proximal micrometer, the fiber and piston move away from the lens and compress a spring that rests on a ridge inside the distal housing. As tension on the fiber is relaxed, the spring provides the restoring force necessary to push the piston and fiber toward the miniature objective. The mechanical focus system is sensitive to frictional forces between the fiber bundle and the semirigid external tubing. To reduce this friction, the fiber is covered by internal tubing made of Teflon.

The mechanical focus mechanism was tested in a similar fashion to that of the pneumatic design de-

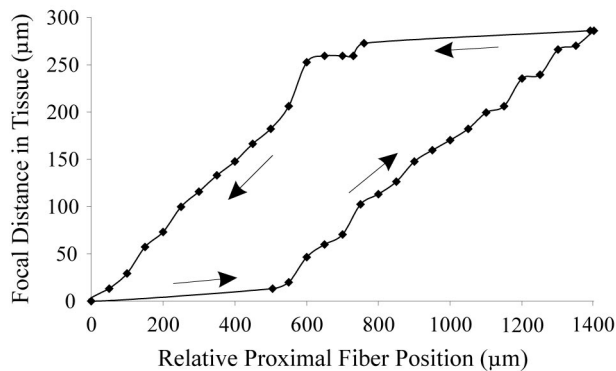


Fig. 9. Measured performance of the mechanical focus mechanism.

scribed in the preceding section. The micrometer in the proximal portion of the focus mechanism was adjusted while the image of the fiber in tissue space was tracked. Figure 9 shows the results for this experiment. The tissue-space measurements were taken in air and then scaled by the refractive index of water to estimate the penetration depth in tissue. It is clear from the data that the focus extent of the mechanical assembly exceeds the imaging depth specification of the confocal microendoscope, which is designed to operate over a 200- $\mu\text{m}$  depth range in the tissue.

The mechanical focus mechanism suffers from significant hysteresis. However, motion is fairly linear and repeatable. As with the pneumatic design, a trained user can quickly scan past the flat hysteresis regions and achieve reliable relative focus control. It is possible to achieve fairly accurate absolute measurements of depth by starting at the tissue surface and scanning in one direction into the tissue. The focal position in the tissue is stable with respect to time but does move slightly as the catheter is repositioned significantly. However, this movement should not be a problem since focusing can be performed again after the catheter is repositioned. As with the pneumatic design, the lateral position of the image is extremely stable with respect to focus. The mechanical focus version of the confocal microendoscope has been successfully and reliably used to image various animal and human tissue samples.

#### 4. Results and Discussion

Figure 10 shows the catheter of the confocal microendoscope routed through the instrument channel of an Olympus CF-100L colonoscope. Figure 10(c) is a still frame captured from the video signal collected by the colonoscope. In this frame, the confocal microendoscope is seen imaging the intestine of a rat. In practice, the wide field of view of the colonoscope will be used to navigate to a suspected site of disease. Then the confocal microendoscope will be extended and pressed against the tissue to provide a microscopic view of the tissue under observation. Ideally, the live images collected by the microendoscope will supply the clinician with the information necessary

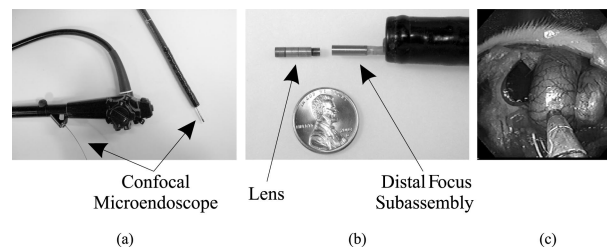


Fig. 10. (a) Confocal microendoscope in the instrument channel of an Olympus CF-100L colonoscope. (b) Detail of the optomechanical components of the catheter. (c) Still frame captured from video collected by the colonoscope and of the microendoscope imaging rat intestine.

to diagnose the state of disease. If a traditional biopsy is warranted, the confocal microendoscope can be removed from the instrument channel and replaced with a biopsy device. Some endoscopes have dual instrument channels, which would be ideal for the confocal microendoscope, as the second instrument channel could be used to deliver dye or to collect biopsy samples or to perform both these functions.

The confocal microendoscope has been used to image *in vivo* and *ex vivo* animal models as well as excised human tissues. Initial applications for the system have concentrated on diagnosing diseases of the gastrointestinal and female reproductive systems. To explore these applications, we have developed close collaborations with physicians who can supply us with human tissue samples. All tissues were collected under protocols approved by the Institutional Review Board of the University of Arizona. To date, the confocal microendoscope has imaged the following excised human tissues: cervix, uterus, ovary, esophagus, stomach, pancreas, and colon. In most cases, the tissue was imaged within 1 h of resection. All images presented here are of tissues stained with acridine orange,<sup>25</sup> which is a vital nucleic acid fluorescent dye that intercalates with DNA and RNA. Acridine orange is efficiently excited by the 488-nm line of an argon-ion laser and has dual emission spectra peaks at 525 and 650 nm when bound to DNA and RNA, respectively. Roughly 100  $\mu\text{l}$  of 330  $\mu\text{M}$  dye is washed over the tissue immediately prior to imaging. Acridine orange is inherently cytotoxic because it intercalates with nucleic acids in live cells. However, topical application of extremely small quantities of dye may not be harmful to humans. *In vivo* fluorescence imaging with exogenous dyes is a relatively new field that will require significant research to develop fluorescent dyes suitable for use in humans.

Figure 11 shows two images obtained with the confocal microendoscope of excised human ovary from different patients. Both were diagnosed as normal ovarian tissue by use of standard histopathology methods. Figure 11(a) shows a regular distribution of densely packed cells characteristic of the surface epithelial layer. Figure 11(b) shows the relatively elongated and loosely packed cells indicative of the underlying stroma. The stroma was clearly visible

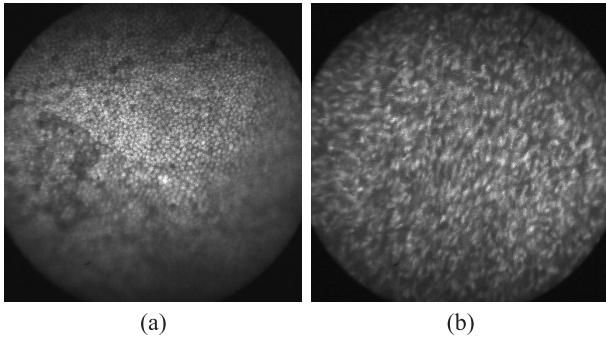


Fig. 11. Excised human ovarian tissue imaged with the confocal microendoscope. (a) Normal epithelial layer. (b) Normal stromal layer. Tissue in (a) and in (b) are from separate patients.

in this case because the epithelial layer had been accidentally scraped off during handling of the tissue. The epithelium is a thin fragile layer that can be damaged without careful tissue handling. This layer should remain intact when the confocal microendoscope is used *in vivo* because the tissue will be imaged with minimal handling.

Figure 12(a) shows diseased human ovary imaged with the confocal microendoscope. Figure 12(b) is a histology image from a similar location on the ovary. The diagnosis for this tissue was cystic papillary carcinoma. An effort was made to match the location of the histology image to the confocal image, but exact registration is difficult. In general, histology and confocal microendoscope images are within 1 mm of each other. We have found that this is adequate for a qualitative correlation of the results.

The two images presented in Fig. 12 are orthogonal views of the same sample. In standard histology, tissue is sliced perpendicular to the surface to produce a cross-sectional view. The confocal microendoscope captures images *en face* and as such, it is impossible to make a direct correlation between the images produced by the two systems. However, it is still clear that there are significant differences between the cancerous tissue of Fig. 12(a) and the normal tissues presented in Fig. 11. By matching confocal microendoscope images to histology, we hope

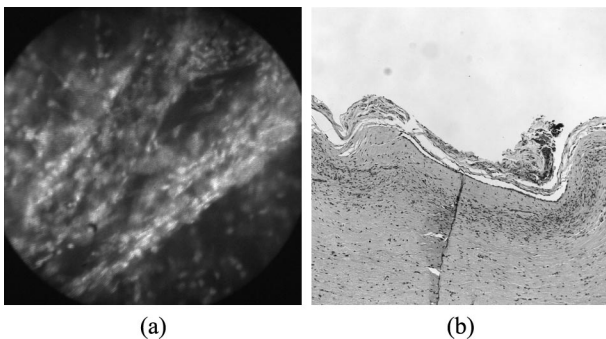


Fig. 12. Excised human ovarian tissue. (a) Confocal microendoscope view. (b) Histology image from a nearby region. This patient was diagnosed with cystic papillary carcinoma.

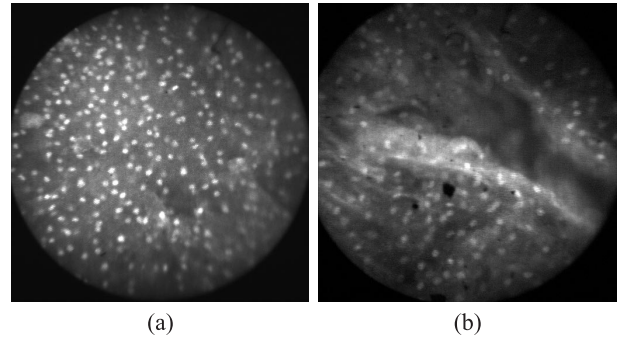


Fig. 13. (a) Healthy excised human cervical tissue and (b) healthy esophageal tissue excised from a patient diagnosed with Barrett's esophagus.

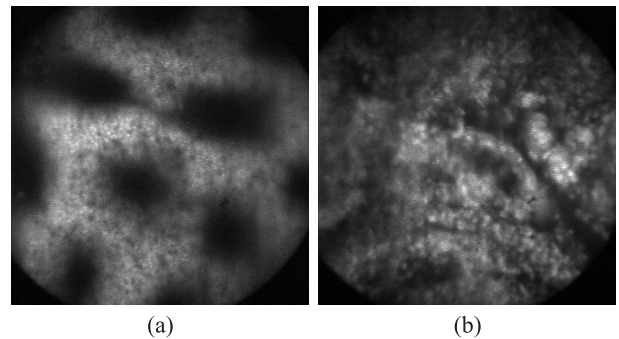


Fig. 14. Excised human colon tissue imaged with the confocal microendoscope. (a) Normal tissue. (b) Tumor region from same patient.

to determine features in the confocal images that identify pathology.

Figure 13(a) shows an image of excised human cervix. The uniform punctate pattern of nuclei is characteristic of healthy cervical tissue, a finding that was supported by histology. Figure 13(b) shows an example of excised human esophagus. This image shows relatively sparse and punctate nuclei but also depicts the slightly undulated surface of the esophagus. This tissue was excised from a patient diagnosed with Barrett's esophagus. However, this particular tissue sample was extracted from a region in the upper portion of the esophagus and was histologically diagnosed as normal.

Figure 14 shows two images of excised human colon. The dark regions in Fig. 14(a) correspond to crypts that extend several hundred micrometers below the surface of the colon. The regular repetitive nature of these crypts is indicative of healthy tissue. Figure 14(b) was taken from a large tumor in the same colon where the normal pattern of crypts is not observed. This example and others suggest that the confocal microendoscope will be able to differentiate healthy from diseased tissue.

## 5. Conclusion

Results with *ex vivo* tissue suggest that the confocal microendoscope with the new 3-mm diameter catheter will produce images of sufficient quality to assist

in the diagnosis of disease. Images of the cervix, ovary, esophagus, and colon presented show significant detail that should aid *in vivo* identification of pathology. The new catheter for the confocal microendoscope may be used on its own or inserted through the instrument channel of a commercial endoscope. The new miniature distal objective has demonstrated nearly diffraction-limited performance allowing high-resolution optical sectioning in tissue. The pneumatic and mechanical focus mechanisms provide precision control of the axial image location in tissue.

The authors thank Jose Sasian for his help with the lens design and Doron Lean and Leo Bartik for their help in the laboratory. Human tissues were provided through clinical collaborations with Molly Brewer and Francisco Garcia at the Arizona Health Sciences Center. This research was supported by NIH grants CA73095 and CA95060 and Arizona Disease Control Research Commission grant 9711.

## References

1. American Cancer Society, "Cancer Facts & Figures 2004" (American Cancer Society, Atlanta, Ga., 2004), <http://www.cancer.org>.
2. M. Minsky, "Microscopy apparatus," U.S. patent 3,013,467 (19 December 1961).
3. T. Wilson, *Confocal Microscopy* (Academic, London, 1990).
4. B. R. Masters, D. J. Aziz, A. F. Gmitro, J. H. Kerr, T. C. O'Grady, and L. Goldman, "Rapid observation of unfixed, unstained human skin biopsy specimens with confocal microscopy and visualization," *J. Biomed. Opt.* **2**, 437–445 (1997).
5. M. Rajadhyaksha, M. Grossman, D. Esterowitz, R. H. Webb, and R. R. Anderson, "*In vivo* confocal scanning laser microscopy of human skin: melanin provides strong contrast," *J. Invest. Dermatol.* **104**, 946–952 (1995).
6. W. M. Petroll, J. V. Jester, and H. D. Cavanagh, "Quantitative three-dimensional confocal imaging of the cornea *in situ* and *in vivo*: system design and calibration," *Scanning* **18**, 45–49 (1996).
7. C. J. Koester, J. D. Auran, H. D. Rosskothan, G. J. Florakis, and R. B. Tackaberry, "Clinical microscopy of the cornea utilizing optical sectioning and a high-numerical-aperture objective," *J. Opt. Soc. Am. A* **10**, 1670–1679 (1993).
8. R. Juskaitis, T. Wilson, and T. F. Watson, "Real-time white light reflection confocal microscopy using a fibre-optic bundle," *Scanning* **19**, 15–19 (1997).
9. T. Collier, P. Shen, B. De-Pradier, S. Kung Bin, R. Richards-Kortum, A. Malpica, and M. Follen, "Near real time confocal microscopy of amelanotic tissue: dynamics of acetowhitening enable nuclear segmentation," *Opt. Express* **17**, 40–48 (2000), <http://www.opticsexpress.org>.
10. R. H. Webb and F. J. Rogomentich, "Microlaser microscope using self-detection for confocality," *Opt. Lett.* **20**, 533–535 (1995).
11. D. L. Dickensheets and G. S. Kino, "Micromachined scanning confocal optical microscope," *Opt. Lett.* **21**, 764–766 (1996).
12. G. J. Tearney, R. H. Webb, and B. E. Bouma, "Spectrally encoded confocal microscopy," *Opt. Lett.* **23**, 1152–1154 (1998).
13. W. McLaren, P. Anikijenko, D. Barkla, T. P. Delaney, and R. King, "*In vivo* detection of experimental ulcerative colitis in rats using fiberoptic confocal imaging (FOCI)," *Dig. Dis. Sci.* **46**, 2263–2276 (2001).
14. J. Knittel, L. Schnieder, G. Buess, B. Messerschmidt, and T. Possner, "Endoscope-compatible confocal microscope using a gradient index-lens system," *Opt. Commun.* **188**, 267–273 (2001).
15. K. B. Sung, C. Liang, M. Descour, T. Collier, M. Follen, and R. Richards-Kortum, "Fiber-optic confocal reflectance microscope with miniature objective for *in vivo* imaging of human tissues," *IEEE Trans. Bio-Med. Eng.* **49**, 1168–1172 (2002).
16. A. F. Gmitro and D. Aziz, "Confocal microscopy through a fiber-optic imaging bundle," *Opt. Lett.* **18**, 565–567 (1993).
17. A. R. Rouse and A. F. Gmitro, "Multispectral imaging with a confocal microendoscope," *Opt. Lett.* **25**, 1708–1710 (2000).
18. Y. S. Sabharwal, A. R. Rouse, L. Donaldson, M. F. Hopkins, and A. F. Gmitro, "Slit-scanning confocal microendoscope for high-resolution *in vivo* imaging," *Appl. Opt.* **38**, 7133–7144 (1999).
19. Sumitomo Electric, 21221 S. Western Avenue, Suite 200, Torrance, Calif. 90501.
20. R. Kingslake, *Lens Design Fundamentals* (Academic, New York, 1978).
21. P. Rudolph, "Object glass," U.S. patent 576,896 (9 February 1897).
22. Optics Technology, 3800 Monroe Avenue, Pittsford, N.Y. 14534.
23. J. D. Gaskill, *Linear Systems, Fourier Transforms, and Optics* (Wiley, New York, 1978).
24. North American Latex, P.O. Box 56062, Vancouver, British Columbia, Canada V5L 5E2.
25. Molecular Probes, 29851 Willow Creek Road, Eugene, Ore. 97402.